Nanoscale Res Lett (2009) 4:699–704
DOI 10.1007/s11671-009-9302-1

NANO EXPRESS

Highly Uniform Epitaxial ZnO Nanorod Arrays for Nanopiezotronics

J. Volk · T. Nagata · R. Erdélyi · I. Bársony · A. L. Tóth · I. E. Lukács · Zs. Czigány · H. Tomimoto · Y. Shingaya · T. Chikyow

Received: 14 January 2009 / Accepted: 24 March 2009 / Published online: 7 April 2009

Abstract Highly uniform and c-axis-aligned ZnO nanorod arrays were fabricated in predefined patterns by a low temperature homoepitaxial aqueous chemical method. The nucleation seed patterns were realized in polymer and in metal thin films, resulting in, all-ZnO and bottom-contacted structures, respectively. Both of them show excellent geometrical uniformity: the cross-sectional uniformity according to the scanning electron micrographs across the array is lower than 2%. The diameter of the hexagonal prism-shaped nanorods can be set in the range of 90–170 nm while their typical length achievable is 0.5–2.3 μm. The effect of the surface polarity was also examined, however, no significant difference was found between the arrays grown on Zn-terminated and on O-terminated face of the ZnO single crystal. The transmission electron microscopy observation revealed the single crystalline nature of the nanorods. The current–voltage characteristics taken on an individual nanorod contacted by a Au-coated atomic force microscope tip reflected Schottky-type behavior. The geometrical uniformity, the designable pattern, and the electrical properties make the presented nanorod arrays ideal candidates to be used in ZnO-based DC nanogenerator and in next-generation integrated piezoelectric nano-electromechanical systems (NEMS).

J. Volk (✉) · R. Erdélyi · I. Bársony · A. L. Tóth · I. E. Lukács · Zs. Czigány
Research Institute for Technical Physics and Materials Science, Konkoly Thege Miklós út 29-33, 1121 Budapest, Hungary
e-mail: volk@mfa.kfki.hu

J. Volk · T. Nagata · H. Tomimoto · Y. Shingaya · T. Chikyow
National Institute for Materials Science, 1-1 Namiki, Tsukuba, Ibaraki 305-0044, Japan

Keywords Aqueous chemical growth · Vertical nanowire · Nanogenerator · NEMS · Piezoelectricity · Rod-type photonic crystal

Introduction

Vertically aligned ZnO nanorods (NRs) and nanowires (NWs) are attracting much interest for several applications such as nanophotonics [1, 2], dye-sensitized solar cells [3, 4], electron field emitters [5, 6], surround-gate field effect transistors [7], and nanopiezotronics [8]. A number of preparation methods by high temperature vapor transport [9] and low temperature chemical synthesis [10, 11] were developed. For comparison, the NR arrays can be classified from several aspects: physical and geometrical properties of the individual building blocks and their uniformity in length, in diameter, and in axis-to-substrate angle. The NRs/NWs can be distributed either randomly or in a well-defined way. The above applications require different kinds of nanostructures concerning their geometrical parameters. For instance, photonic crystals with well-defined defects are of importance in nanophotonics [12, 13]. Another demanding application is the construction of ZnO NW-based DC current generator, where the NWs convert the mechanical energy of a vibrating Pt-coated, zig-zag-shaped electrode to electric energy by exploiting the piezoelectric nature of ZnO [14]. Even for nanosensors, however, the generated power density ($\sim$80 nW/cm^2) should be significantly increased. As Liu et al. [15] have pointed out the output voltage of the system, being now typically in the order of $\sim$10 mV, can be drastically improved by increasing the number of the active NW-s, i.e., the ones which are in continuously contact with the zigzag top electrode. Therefore, two approaches were proposed:

improving the uniformity of the NWs on one hand and patterning the array according to the dimension and shape of the top electrode. Vertical ZnO nanoarrays arranged in a designed pattern were recently produced by a few groups using different techniques [16, 17], however, either the geometrical non-uniformity of the NWs or the low density of the vertical microcrystals (~ 1 NR/μm^2) makes their use in nanogenerator application difficult. Moreover, if the nanostructure is produced by vapor–liquid–solid (VLS) method the metal catalyst droplet on the top of the NW can hinder the formation of the required Schottky contact at the top electrode/NW interface.

Here, we demonstrate alternative fabrication routes which fulfill all the above crucial requirements by providing highly uniform, crystallographically oriented NRs in the 100-nm diameter range, in predefined, dense patterns. Our method benefits of the catalyst free, low temperature epitaxial growth, and the direct writing nanolithography. We have tried two options for the formation of NR arrays. In the first, the desired nucleation pattern was drawn in a polymethyl-methacrylate (PMMA) layer, which was subsequently removed resulting in an all-ZnO structure. In the second route, the nucleation pattern was realized in a hard metal coating; therefore, the fabricated NRs were electrically contacted at the anchoring surface.

Experimental

All ZnO NR Array

The process flow for the fabrication of all-ZnO NR arrays is shown in Fig. 1a–d. At first, the Zn- and O-terminated single crystal ZnO wafers were washed ultrasonically in acetone, ethanol, and deionized water, which was followed by a thermal-annealing step in a quartz tube at 1,050 °C for 8 h in oxygen atmosphere. In order to prevent the sublimation of Zn, the substrates were placed between yttrium stabilized zirconia (YSZ) wafers before annealing. The 250-nm-thick PMMA resist layer was exposed by e-beam lithography in an Elionix ELS-7500EX instrument (Fig. 1b). Circular spots of different (50–100 nm) diameters arranged in a triangular (TRI) or honeycomb (HC) lattice were generated. They behave as active centers for ZnO nanostructure growth in the PMMA layer. The growth was effected by the aqueous chemical growth technique (Fig. 1c). The aqueous bath contained the same (4 or 40 mM) molar amount of zinc nitrate hexahydrate ($Zn(NO_3)_2 \cdot 6H_2O$) and hexamethylene tetramine ($(CH_2)_6N_4$). During the ZnO nanostructure growth, the specimen was mounted upside-down on a polytetrafluoroethylene (PTFE) sample holder. The nanocrystal growth was carried out—without an electric field applied—in a multipurpose oven for 1–3.5 h periods at a set temperature of 85 °C. However, due to the high heat capacity of the glass container and the dry atmosphere, the warming up was relatively slow: the bath temperature reached 80 and 82 °C after 2 and 3 h, respectively. Following slow cooling, the sample was thoroughly washed in de-ionized water and purged in nitrogen. Afterward, the PMMA layer was removed in acetone. This step also helps to lift-off the parasitic ZnO debris formed in the solution volume (Fig. 1d).

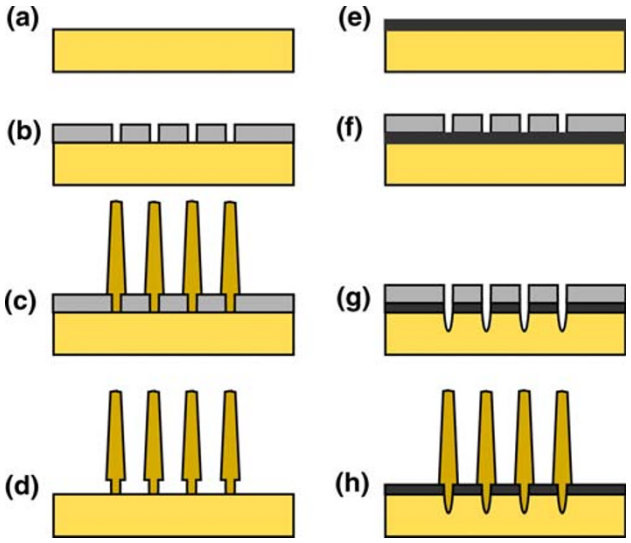

Fig. 1 Schematic process flow of all-ZnO (**a**–**d**) and anchored (**e**–**h**) nanorod arrays. The processing steps for all-ZnO structure are: surface treatment of ZnO substrates (**a**), pattern generation in PMMA by e-beam lithography (**b**), chemical nanowire growth (**c**), and PMMA removal (**d**). Processing steps for the anchored ZnO array are: Ru thin film deposition (**e**), e-beam lithography (**f**), Ar^+ ion milling (**g**), and chemical nanorod growth after PMMA removal (**h**)

Anchored NR Array

Nanorods grown through a hard metal mask obtained by Ar-ion milling are anchored in the single crystal substrate in the recessed dips etched during metal milling. Thereby the fabrication of arrays of electrically contacted NRs is achieved. The process shown in Fig. 1e–h is partly similar to that of the previously introduced all-ZnO arrays. However, here the surface treatment process of ZnO substrate was followed by the deposition of a 30-nm-thick, high-quality Ru layer by using ion-beam sputtering [18] (Fig. 1e). The pattern was formed first in PMMA by e-beam lithography (Fig. 1f) and was transferred into the hard metal film by Ar^+ ion milling (Fig. 1g). For the NR synthesis, the same chemical growth method was used as for the all-ZnO arrays (Fig. 1h). The preparation condition details for both all-ZnO and anchored arrays are summarized in Table 1.

Table 1 Summary of the growth parameters and the obtained nanorod dimensions

Type	Surface polarity (Zn/O)	Hole diameter (nm)	Inter-rod distance (nm)	Lattice type	Nanorod density (NR/μm^2)	Growth concentration (mM)	Growth time (min)	Feret's diameter (nm)	Length (μm)	Figures
All-ZnO	O	75	263	HC	11	4	180	170	1.6	2a
All-ZnO	Zn	100	200	TRI	29	4	60	125	0.5	2b
All-ZnO	O	80	200	TRI	29	4	180	94	1.0	2c
All-ZnO	Zn	100	350	HC	6	40	130	–	3.5	2d
Anchored	Zn	100	350	HC	6	4	270	150	2.2	3a
Anchored	Zn	75	263	HC	11	4	270	135	2.3	3b
Anchored	Zn	50	175	HC	25	4	270	90	2.3	3c

Characterization Methods

The obtained nanostructures were visualized by a Hitachi S4800 field emission scanning electron microscope (FE-SEM). Transmission electron microscope (TEM) images were obtained by a 200 kV JEOL JEM-2010 instrument. The electrical characterization of the individual NWs was carried out in air by conductive AFM technique by means of a SII NanoTechnology Inc., SPA-400 instrument equipped with Keithley 4200-SCS semiconductor parametric analyzer. The spring constant and resonant frequency of the used Au-coated cantilever is 1.4 N/m and 26 kHz, respectively.

Results and Discussion

The SEM images of the all-ZnO arrays fabricated at optimized conditions are shown in Fig. 2a–c. The c-axis-oriented NRs show hexagonal cross section, which are according to the crystal orientation of the substrate collectively aligned to each other. The sidewalls of the prism-shaped rods correspond to the most stable non-polar $\{1\bar{1}00\}$ faces. Note the ~250 nm high bottleneck-shaped part at the bottom of the nanocrystals in Fig. 2a, which was formed inside the cylindrical hole developed in the PMMA layer. We have found that by changing the template geometry, the diameter and the length of the NRs can be tuned in the range of 90–170 nm and 0.5–2.3 μm, respectively. Detailed geometrical parameters for every specimen are summarized in Table 1. The perpendicularly standing NRs reflect excellent geometrical uniformity. According to the image analysis done on the FESEM image (pixel size of 1.4 nm) shown in Fig. 2b, the average Feret's diameter is 125 ± 2.1 nm. This is the diameter of a circle having the same area as the hexagonal cross section of the object. It corresponds to a relative deviation of ~1.6% (Fig. 2b inset). We have tried the same growth conditions on Zn- and O-polar ZnO surfaces, but no significant difference

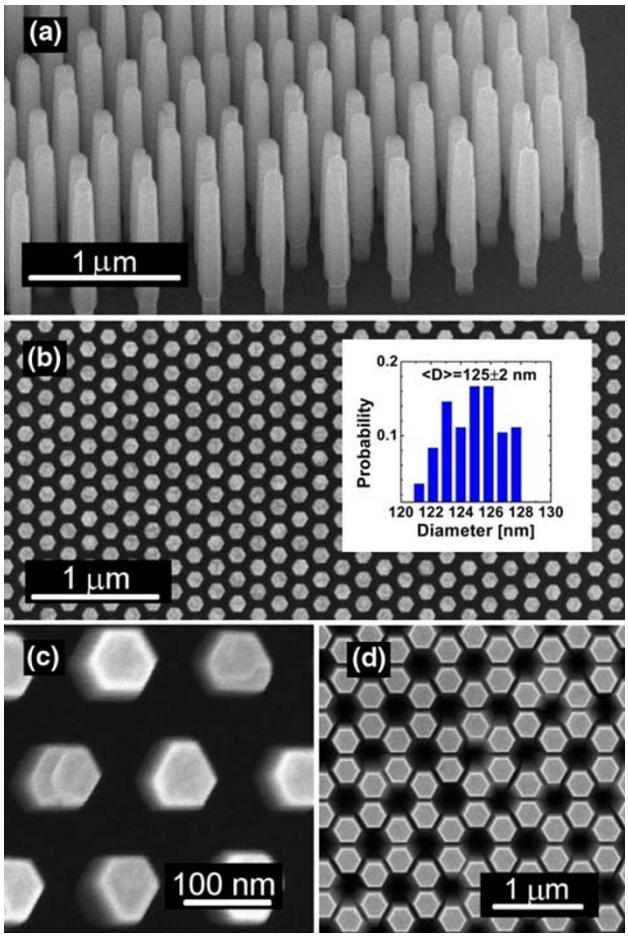

Fig. 2 FESEM images on all-ZnO nanorod arrays prepared by soft-masking method in honeycomb (**a**, **d**) and on triangular (**b**, **c**) arrangements. The single crystal nanorods have hexagonal cross-sections; the uniformity of diameter can be <2% (b inset). When the concentration of the growth solution is increased to 40 mM, a coalescence of nanorods is observed (d)

was found in the obtained arrays. A typical example observed during the optimization of the growth parameters is inserted in Fig. 2d. When the concentration in the growth solution is increased to 40 mM, the growing NRs coalesce at their non-polar sides to form a contiguous network.

Anchored, i.e., metal back contacted arrays show similar geometrical features as the all-ZnO structures (Fig. 3a, b). Here, we have also downscaled the pattern: the densest array had an rod-to-rod distance of 175 nm, which in HC lattice corresponds to a NR density of 25 NR/μm. However, in the case of high aspect ratio (~26:1) and short rod-to-rod distance, a self-attraction of NR tips occurs (Fig. 3c).

Similar phenomenon was described by other groups, as well, albeit they used high temperature vapor transport methods. Wang et al. [19] explained the self-attraction by the accumulated Coulomb charges at the NR/Au catalyst droplet interface when charged by the primary electrons during SEM observation. Han et al. [20] have also observed self-attracted NWs prepared by catalyst-free vapor–solid (VS) preparation method. Therefore, the charging cannot be ascribed to the presence of catalysts.

In our case, the NR tip attachment can be attributed to surface tension of water during the drying process, as it was described by Segawa et al. [21] for hybrid organic–inorganic NR. We believe that further down-scaling is limited mainly by the resolution of our e-beam lithography facility rather than by growth kinetics.

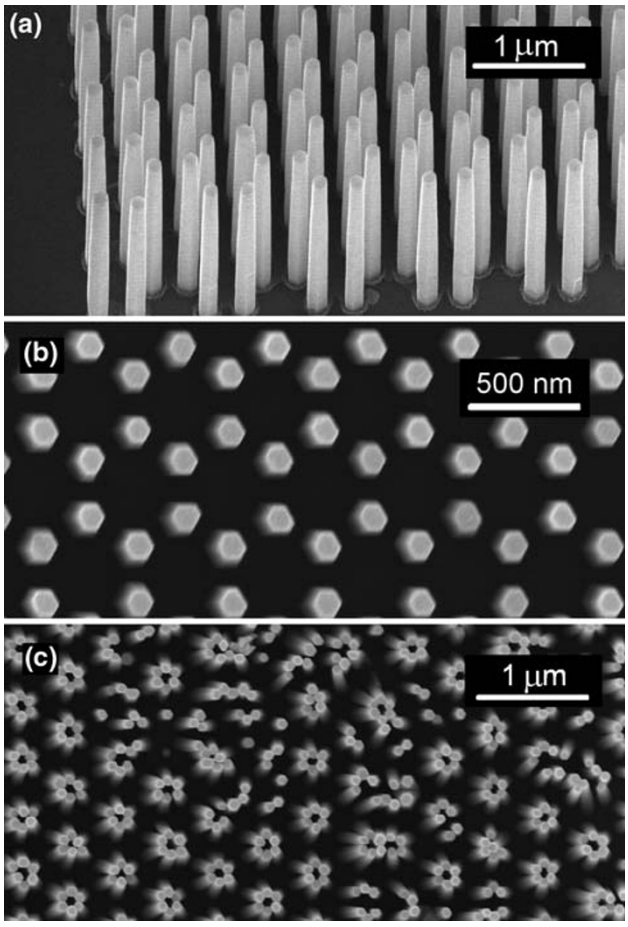

Fig. 3 Perspective view (**a**) and top view (**b**) FESEM images on bottom contacted, anchored ZnO nanorods prepared by hard-mask method. The arrays show similar geometrical features as all-ZnO nanostructures. When the aspect ratio is high, during the drying process (**c**) the nanorods attach to each other at their tips

In Fig. 4a, the cross-sectional FESEM image of the so-called anchored-type NRs is provided. The height of the nanostructures is highly uniform. The arrows on top and bottom mark the characteristic diameter of the rods being ca. 165 ± 10 nm and 250 ± 15 nm, respectively. The development of this taper is the effect of the finite growth rate on the nonpolar faces of the sidewalls. Figure 4b reflects the anomaly encountered during ion-milling of the base-metal film (Ru) through the PMMA holes formed by e-beam lithography. After the removal of the PMMA mask, a cylindrical object is left surrounding the ion-milled hole in the metal. This cylinder is composed of sputtered residues originating from the Ru-film, mixed with ZnO from the underlying substrate and polymers formed from PMMA components. A schematic cross section of the structure after ion-milling, but before PMMA removal, is shown in Fig. 4c. This is determining the starting diameter of the growth within the anchor. The hexagonal faceting forms outside of this cylinder. That gives rise to the neck observed on the bottom of the NRs in Fig. 4a.

The TEM observations revealed that both all-ZnO and anchored, contacted NRs are wurtzite type single crystals of high quality (Fig. 5), where the rotational axis is parallel to the [0001] direction.

The electrical properties of the individual NRs in Fig. 3a were characterized by the conductive AFM technique. We found that an increased contact force was required to obtain a reproducible result. This can be ascribed to the effect of the condensates on the mantle surface of the NRs. The obtained current–voltage curve indicates Schottky-type

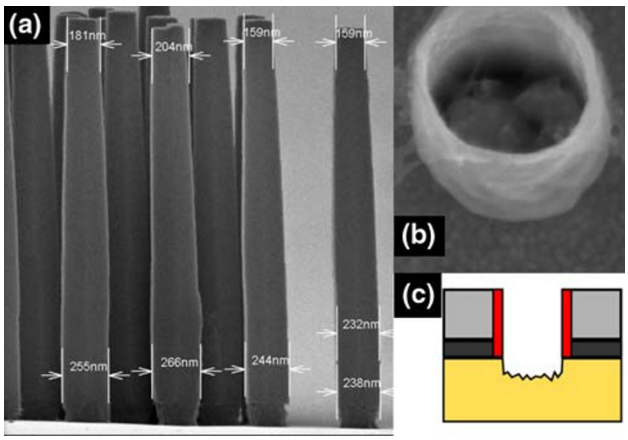

Fig. 4 FESEM image of the cross section of anchored-type ZnO nanorods with indication of the size-distribution (**a**), the parasitic ring remaining after removal of the PMMA mask (**b**), and from the Ar^{+}-ion milled structure shown in the sketch in cross section (**c**)

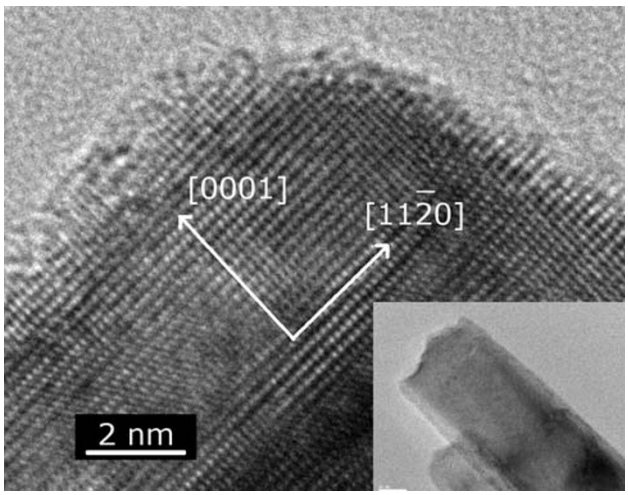

Fig. 5 The TEM observation reveals the single crystalline nature of the nanorods. The fast growing [0001] crystallographic direction is parallel to the longitudinal axis

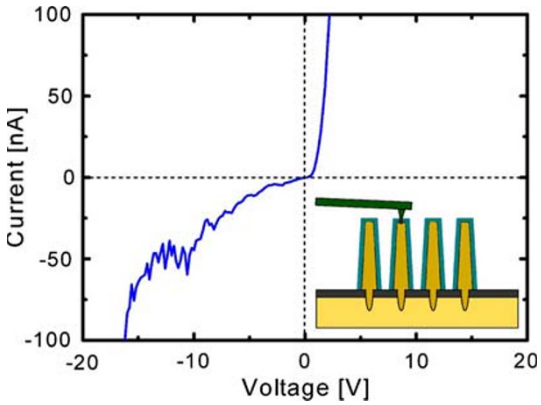

Fig. 6 Current–voltage characteristic recorded on an individual nanorod by conductive AFM. In order to obtain reproducible results in air increased contact force is required, which can be ascribed to the condensate formation on the nanorods (*inset*)

behavior (Fig. 6), which can be originated either from the contact between probe-tip and NR-tip or from the collar-shaped ZnO/Ru interface at the bottom of the NR. However, as it was shown earlier [18] and found here as well, the Ru/single crystal ZnO interface-contact has Ohmic character. Therefore, the Au/ZnO NR contact is responsible for the observed rectifying behavior.

In order to correctly describe the electrical behavior by an equivalent circuit and to separate the contributions of contact resistance, internal resistance of the NR, surface conductance, and piezoelectricity induced Schottky barrier height change, a refinement of the measurement technique and further systematic investigation is required. Still, in our work the successful formation of a rectifying Schottky contact between ZnO NR and the measuring tip could reproducibly be obtained. This was pointed out by Liu et al. [22] to be a necessary requirement for the operation of the DC nanogenerator with vibrating top contact.

Conclusions

We have demonstrated that by using homoepitaxial chemical growth method highly uniform, single crystalline NR arrays arranged in a predefined pattern can be prepared. By changing the growth parameters, diameter and length of the NRs can be tuned in the range of 90–170 nm and 500 nm–2.3 μm, respectively. The monodispersity of the diameter of single crystalline NRs can be <2% by maintaining an excellent uniformity in the longitudinal dimension. We exploited two alternative synthesis routes using soft and hard under-layer to obtain all-ZnO and metal contacted, anchored NR arrays, respectively. The former one can be a promising candidate for nanopillar-based photonic crystals, especially if a refractive index contrast between the NR and the ZnO substrate is realized. On the other hand, anchored NR arrays contacted on the bottom are promising structures for nanopiezotronics. The arrays show excellent uniformity in length and the dense pattern ($\sim$30 NR/μm^2) can be adjusted to the top vibrating electrode of the nanogenerator. Thereby a significant improvement in the output voltage, hence a more efficient energy harvesting can be predicted.

Acknowledgments This work was supported by the "Nanotechnology Network Project" of the Ministry of Education, Culture, Sports, Science and Technology (MEXT) in Japan, and by the Hungarian Fundamental Research Found (OTKA) under contract PD 77578. The authors are grateful to Prof. Y. Bando for the valuable suggestions and to Mr. Y. Misawa, Mr. S. Hara, Mr. K. Tamura, and Mr. A. Ohi for professional help with sample preparation.

References

1. M.H. Huang, S. Mao, H. Feick, H. Yan, Y. Wu, H. Kind, E. Weber, R. Russo, P. Yang, Science **292**, 1897 (2001). doi:10.1126/science.1060367
2. R. Konenkap, R.C. Word, C. Schlegel, Appl. Phys. Lett. **85**, 6004 (2004). doi:10.1063/1.1836873
3. M. Law, L.E. Greene, J.C. Johnson, R. Saykally, P. Yang, Nat. Mater. **4**, 455 (2005). doi:10.1038/nmat1387
4. J.B. Baxter, E.S. Aydil, Appl. Phys. Lett. **86**, 053114 (2005). doi:10.1063/1.1861510
5. Y.-K. Tseng, C.-J. Huang, H.-M. Cheng, I.-N. Lin, K.-S. Liu, I.-C. Chen, Adv. Funct. Mater. **13**, 811 (2003). doi:10.1002/adfm.200304434
6. A. Wei, X.W. Sun, C.X. Xu, Z.L. Dong, M.B. Yu, W. Huang, Appl. Phys. Lett. **88**, 213102 (2006). doi:10.1063/1.2206249
7. H.T. Ng, J. Han, T. Yamada, P. Nguyen, Y.P. Chen, M. Meyyappan, Nano Lett. **4**, 1247 (2004). doi:10.1021/nl049461z
8. Z.L. Wang, Adv. Mater. **19**, 889 (2007). doi:10.1002/adma.200602918
9. Z.Y. Fan, J.G. Lu, J. Nanosci, Nanotechnology **5**, 1561 (2005). doi:10.1166/jnn.2005.182

10. L. Vayssieres, K. Keis, S.-E. Lindquist, A. Hagfeldt, J. Phys. Chem. B **105**, 3350 (2001). doi:10.1021/jp010026s
11. B. Liu, H.C. Zeng, J. Am. Chem. Soc. **125**, 4430 (2003). doi:10.1021/ja0299452
12. M. Tokushima, H. Yamada, Y. Arakawa, Appl. Phys. Lett. **84**, 4298 (2004). doi:10.1063/1.1755838
13. S.H.G. Teo, A.Q. Liu, J. Singh, M.B. Yu, G.Q. Lo, Appl. Phys. A: Mater. Sci. Process. **89**, 417 (2007). doi:10.1007/s00339-007-4122-6
14. X. Wang, J. Song, J. Liu, Z.L. Wang, Science **316**, 102 (2007). doi:10.1126/science.1139366
15. J. Liu, P. Fei, J. Zhou, R. Tummala, Z.L. Wang, Appl. Phys. Lett. **92**, 173105 (2008). doi:10.1063/1.2918840
16. J.H. He, J.H. Hsu, C.W. Wang, H.N. Lin, L.J. Chen, Z.L. Wang, J. Phys. Chem. B **110**, 50 (2006). doi:10.1021/jp055180j
17. Y.-J. Kim, C.-H. Lee, Y.J. Hong, G.-C. Yi, Appl. Phys. Lett. **89**, 163128 (2006). doi:10.1063/1.2364162
18. T. Nagata, P. Ahmet, Y.Z. Yoo, K. Yamada, K. Tsutsui, Y. Wada, T. Chikyow, Appl. Surf. Sci. **252**, 2503 (2006). doi:10.1016/j.apsusc.2005.05.085
19. X. Wang, C.J. Summers, Z.L. Wang, Appl. Phys. Lett. **86**, 013111 (2005). doi:10.1063/1.1847713
20. X. Han, G. Wang, L. Zhou, J.G. Hou, Chem. Commun. 212 (2006). doi:10.1039/b512259g
21. H. Segawa, S. Yamaguchi, Y. Yamazaki, T. Yano, S. Shibata, H. Misawa, Appl. Phys. A: Mater. Sci. Process. **83**, 447 (2006). doi:10.1007/s00339-006-3568-2
22. J. Liu, P. Fei, J. Song, X. Wang, C. Lao, R. Tummala, Z.L. Wang, Nano Lett. **8**, 328 (2008). doi:10.1021/nl0728470